HERA Mission LIDAR Mechanical and Optical Design

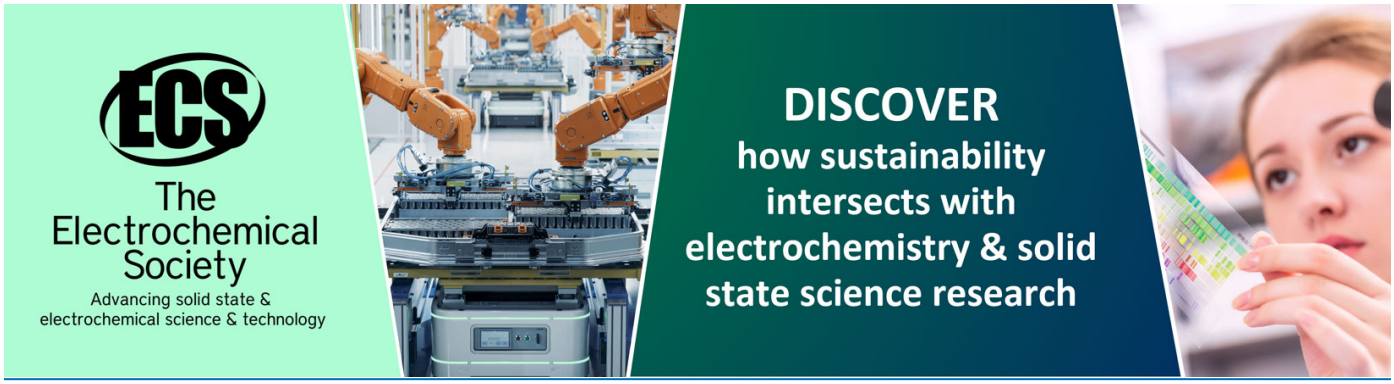

HERA Mission LIDAR Mechanical and Optical Design

Nicole G. Dias[1], Beltran N. Arribas[1], Paulo Gordo[1], Tiago Sousa[2], João Marinho[2], Rui Melicio[3,4], António Amorim[1], Belegante Livio[5]and Patrick Michel[6]

[1]CENTRA, Faculdade de Ciências, Universidade de Lisboa, Lisboa, Portugal
[2]Aerospace Division, EFACEC Power Solutions, São Mamede de Infesta, Porto, Portugal
[3]IDMEC, Instituto Superior Técnico, Universidade de Lisboa, Lisboa, Portugal
[4]ICT, Universidade de Évora, Évora, Portugal
[5]Optoelectronics, National Institute of R&D, Romania
[6]Observatoire de la Côte d'Azur, CNRS, Nice, France
Corresponding author: Rui Melicio; ruimelicio@gmail.com

Abstract. Near-Earth Objects (NEO) are the topic of several research studies, with objects smaller than 1km in size posing the most threats and being the less understood of this scientific domain. The Asteroid Impact and Deflection Assessment (AIDA) mission involves NASA and ESA with the main mission goal to perform and analyze the asteroid deflection using the Kinetic Impactor technique. The mission target is Didymos-B, a moon of a binary asteroid called Didymos. NASA oversees the Double Asteroid Redirection Test (DART probe), and ESA is responsible for HERA probe, that will measure the Dydimos-B deflection caused by the impact. The Light Detection and Ranging (LIDAR), the Radar, the Satellite-to-Satellite Doppler tracking, the Seismometer, and the Gravimeter are instruments integrated into HERA spacecraft. Information synergy between the instruments allows the detailed characterization of the asteroid including internal structure. This experiment allows further understanding and will provide important information to improve the current NEO understanding and modelling. In this paper, scientific advances related to the LIDAR instrument are reported, including the innovative optomechanical design resulting from thermal and mechanical optimizations. The LIDAR has a compact design and needs to withstand extreme conditions, such as radiative and thermal conditions, without compromise its high accuracy measurements. The LIDAR is a time-of-flight altimeter instrument that will measure the distances from the HERA spacecraft to the target. It provides information for a 3D topographic mapping and calculates the asteroid reflectivity. The measurements are to be performed at a distance from 500 m to 14 km while operations such as fly byes or landings remain a possibility.

Keywords. LIDAR, HERA mission, Thermal design, Optomechanical design, NEO

1. Introduction

The AIDA mission is an effort between NASA and ESA, including the DART and HERA missions, respectively. DART's primary goal is to demonstrate the deflection of an asteroid using the kinetic impact technique and HERA is to characterize the deflection caused by the impact. The target, called Didymos-B, is a small object from a binary Near-Earth Asteroid, Didymos [1].

The HERA spacecraft includes several payload instruments, such as the Time-of-Flight (ToF) LIDAR that will measure the distances from the HERA spacecraft to the target. The measurement operations shall be performed a distance from 500 m to 14 km and operations such as fly byes or landing operations are possible.

Previous space missions have deployed analogous instruments for specific requirements. The main challenges of those missions were the operational temperature range, since the LIDARs are directly exposed to space, and the required optical tolerances to maintain the instrument performance (i.e., internal alignment of optics and alignment between receiver and emitter).

Each mission requires a specific LIDAR measurement range, operational temperatures interval, radiation requirements and target objects, making the LIDAR design rather specific.

Since 1970, NASA has been developing laser profilers and scanners, and the Apollo missions [2] were the pioneer for the space-borne altimeters.

In 2003, Hayabusa was launched to explore the asteroid Itokawa. The LIDAR onboard Hayabusa measured distances between 50m to 50km, and provided range information, with meter accuracy, and range rate information at the initial encounter to the asteroid [3].

A year later, in 2004, the Mercury Surface, Space Environment, Geochemistry and Ranging (MESSENGER) spacecraft was launched. The Mercury Laser Altimeter (MLA) was onboard, and it was capable to determine Mercury's surface elevation, liberation, and internal structure. MLA performed range measurements from distances of 800 km at a maximum slant range of 53°, enduring the low planet albedo, the high-IR flux and the solar background of the planet [4].

The Lunar Reconnaissance Orbiter (LRO) spacecraft was launched in 2009, with the Lunar Orbiter Laser Altimeter (LOLA) onboard to "select safe landing sites, identify lunar resources, and study how the lunar radiation environment will affect humans" [5]. A three-dimensional map of the moon, with measurements of surface elevation, slope, and roughness, was made by LOLA, and innovative optical technologies were verified. The LOLA laser transmitter and laser ranging system also contributed to the improvement of the orbit determination of LRO around the Moon [5].

Regarding Hayabusa missions, the LIDAR used were mainly directed to rendezvous and touchdown control [3]. During the Hayabusa2 mission, the LIDAR, apart from measuring ranges, also obtained the albedo's asteroid, by the ratio between the intensity of transmitted and the received laser pulses [6].

The Origins, Spectral Interpretation, Resource Identification and Security Regolith Explorer (OXIRIS-REX) was launched in September 2016 with the aim to return a sample from asteroid 101955 Bennu. The OXIRIS-REX Laser Altimeter (OLA) will measure the asteroid's shape and will provide global maps of slopes [7]. OLA has both long- and short-range transmitters with a measurement rate of 100 Hz for distances above 1km and 10 kHz for smaller distances. A scanning mirror also samples large portions of the asteroid surface in a short time [7].

In this paper, the thermal and optical tolerance requirements are studied, by using radiative and thermo-elastic models simulated on ESATAN-TMS and ANSYS software, respectively. The radiative results were directly used by the thermoelastic models, and the critical values were obtained and assessed according to the tolerance analysis. The paper is structured as follows. Section 2 is about the LIDAR design, Section 3 presents the thermo-mechanical design, Section 4 presents the radiative and thermo-mechanical models, Section 5 outlines conclusions.

2. LIDAR Design

The HERA LIDAR receiver follows a Cassegrain telescope design, as depicted in Figure 1, including a primary mirror, a secondary mirror, a lens and a sensor.

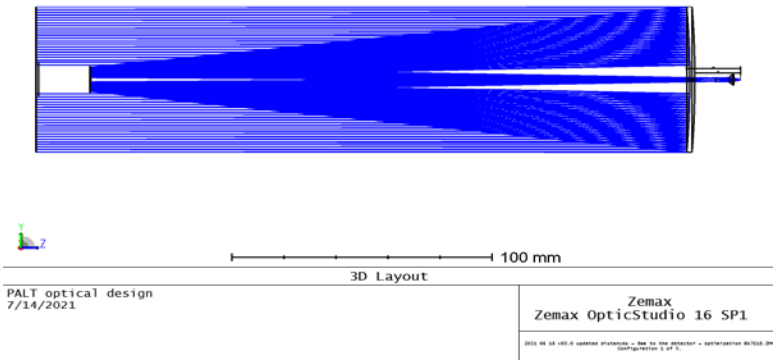

Figure 1. LIDAR Receiver telescope optical design (ZEMAX).

The primary mirror is made of Zerodur with a diameter of 70 mm and is assembled on isostatic bipod mounts to compensate thermal variations. The secondary mirror is also made of Zerodur with a diameter of 14 mm, and it is assembled on a carbon fibre tripod structure.

The emitter has a microchip laser that emits pulses of light at 1535 nm, with a pulse energy of 100 μJ and a pulse width of 2 ns. The radiometric model of this instrument was discussed in [8,9], where the link equation is used to calculate the received pulse energy, which depends on the transmitted laser pulse energy, the emitter and receiver transmittance, the asteroid reflectance, the geometry of the receiver telescope, the distance between LIDAR and the target and the overlap between the emitter and receiver. This equation is important to calculate the critical parameters required for the LIDAR receiver aperture.

An optical tolerance analysis was performed using ZEMAX, which allowed to identify optical tolerance worst offenders. The information retrieved with this analysis defines the optical specifications ranges, such as the distance between mirrors in the LIDAR receiver, and the tilt of the optical elements. These critical parameters must be respected during the operational phase of the mission, making it possible to establish the acceptance thermal tolerance (i.e., optical parts position requirements), that are used in the thermoelastic simulations. The main concern addressed in this paper are the tolerances of the primary mirror tilt, the secondary mirror tilt and the distance between each other. Table 1 presents the critical optical elements tolerances that must be met for all operational ranges.

Table 1. Thermal operation tolerances

Primary mirror (M1)	Tilt (mrad)	∓ 0.03
Secondary mirror (M2)	Distance from primary (mm)	∓ 0.05
	Tilt (mrad)	∓ 0.05
Telescope vs emitter	Angle between emitter and telescope (mrad)	∓ 0.15

3. Thermo-Mechanical Design

This Section focuses on the receiver telescope and electronics box thermal and mechanical design (see Figure 2). The HERA LIDAR is a compact instrument with an overall mass of less than 2 kg. The engineering model of the LIDAR, called HELENA, was addressed in [8,9]. The lessons learned from HELENA demonstrated that it is helpful to optimize the thermal and mechanical design of the LIDAR flight model (PALT). To protect the instrument and minimize the thermal effects, the instrument will be thermal shielded, i.e., protected by a baffle that is covered by MLI (Multi-Layer Insulation). The thermal and radiant environment during operation is the focus of the Section 4.

The thermo-mechanical design was based on the operational tolerances dictated by the optical design (see Figure 1). Regarding the thermal design, as shown in Figure 2, an aluminum baffle was added to the telescope, with an upper ring, with its interior painted in black, and the inner upper part upside in white. The instrument is thermically shielded by MLI and the different subsystems are thermically insulated with thermal washers (see Figure 3). The instrument is at the center of the satellite and therefore it is not possible to use conventional radiators. To maintain the receiver telescope at a lower temperature for the high temperature scenarios, the telescope baffle will act as radiator and optical baffle (for stray light), this double function is an innovative thermal/optical/mechanical implementation. Several approaches of thermal washers' design and baffle implementation were investigated, such as a baffle in the emitter, but were shown not to be required.

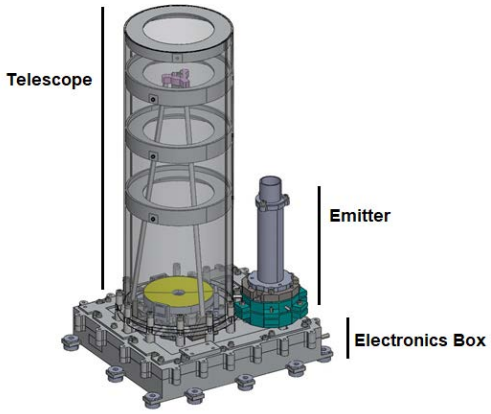

Figure 2. PALT design.

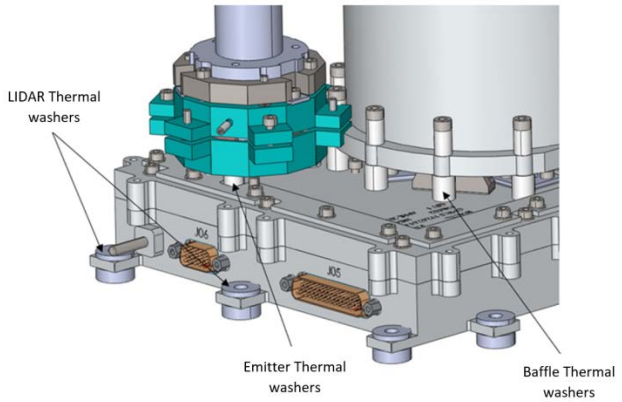

Figure 3. Thermal washers' location.

Several mechanical designs of the electronics box lid were studied. The electronic box lid is the bench plate of the LIDAR optical front-end and minimizing the deformation during the operational temperature range from -30ºC to 50ºC is a critical aspect. Figure 4 shows the first approach of the box design, that was shown not to be sufficient to meet the optical tolerance requirements. After several design iterations, the final box design converged to the model presented in Figure 5 and Figure 6. In this design a layer of cho-therm was used, between the frame and the lid, to allow for a better insulation along the box, and guarantee that the lid does not deform in excess. As shown in Figure 6, the lid is only secured between the preload frame and the main frame to allow for a relatively free deformation. The preload and the frame are fastened by the screws designated in 1, and 2 (Figure 6) to link the frame and the reinforcement, and by 3, that is to connect the frame with the side box.

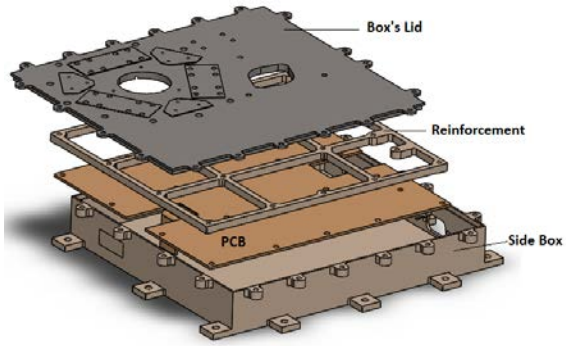

Figure 4. First electronics box design.

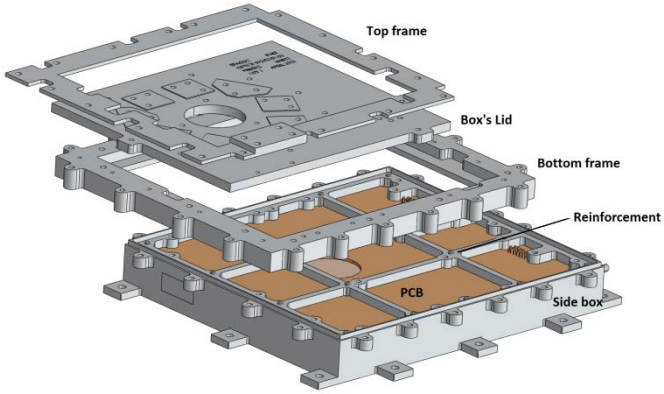

Figure 5. Latest electronics box design.

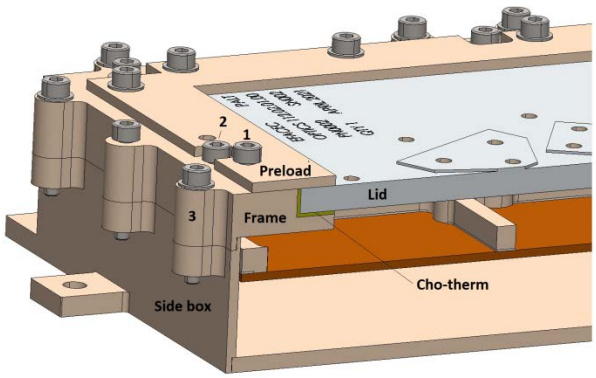

Figure 6. Detail of the lid box assembly.

4. Radiative and Thermo-elastic Models

The thermal and mechanical design of the LIDAR flight model was developed following two parallel approaches: first, a thermal study, including radiation, that was made using ESATAN-TMS (see Figure 7), followed by a thermoelastic analysis on ANSYS (see Figure 8) from the results retrieved from ESATAN-TMS (i.e., LIDAR parts temperatures in different operational scenarios). A conductive heat analysis alone was made to verify both models in software's, i.e., ESATAN-TMS and ANSYS.

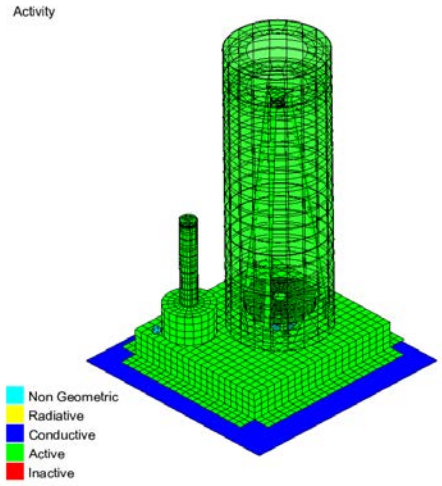

Figure 7. Radiative model on ESATAN-TMS.

Figure 8. Thermoelastic model on ANSYS.

The radiative study cases were only performed by ESATAN. The conductive boundaries are considered in this analysis (the S/C layer condition), together with the radiative conditions. Three different cases were simulated: Hot operational case (Hot op); Cold non-operational case (Cold non-op); Hot non-operational case. Their boundary conditions are summarized in Table 2. The simulations were carried out for the critical scenarios: Hot operational case with a solar angle of 15°; Hot non-operational case with a solar angle of 55°; Cold non-operational case with a solar angle of 0°; Cold operational additional scenario that has the same boundary conditions that the Cold non-operational case. In this paper only the hot operational case with a solar angle of 15° will be presented.

Table 2. Boundary conditions for Radiative simulation

Thermal boundary	Hot op	Cold non-op	Hot non-op
Radiative boundary	-270°C	-270 °C	-270°C
Conductive boundary	50°C	-30°C	65°C
Thermal load	Hot op	Cold non-op	Hot non-op
Solar flux	600W/m²	no solar flux	1320W/m²
Solar angle	worst of range: 0º - 15°		worst of range: 0º - 55°

The orbital conditions correspond to an altitude of 212 km, a RAAN (Right Ascension of the Ascending Node) of 71° and finally an inclination of 90°. The LIDAR will be used for observing the asteroid at approximately 2.5 AU from the sun therefore the radiance was set manually to 600 W/m^2. The additional optical properties like the surface emittance, absorptance and reflectance were defined with EOL (End of Life) values, with a solar declination of 0°, a planet albedo of 0 (since it is an asteroid), and a space temperature of 3 K were used.

The conductive boundary conditions are set on the base of the instrument and the electronic components are dissipating a total of 1.8 W.

The temperature values of the critical components are shown from Figure 9 to Figure 12. The optical and electronic components are within the operational and survival temperature limits.

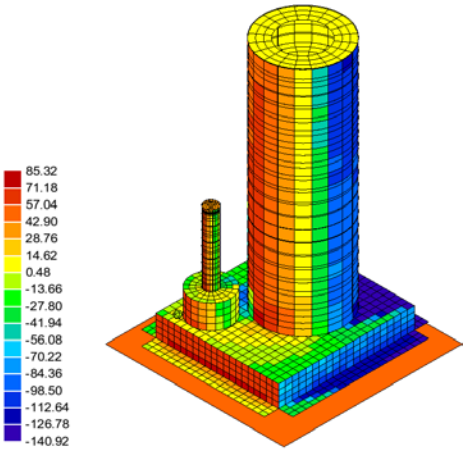

Figure 9. Temperature of PALT including MLI

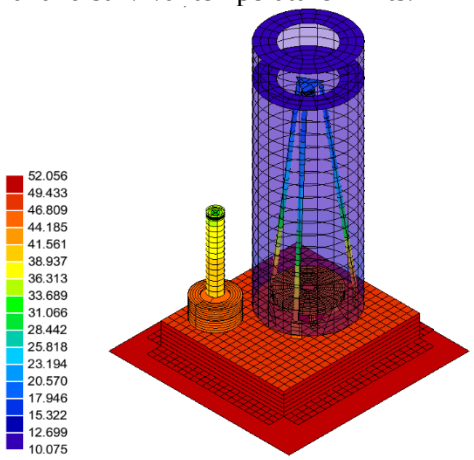

Figure 10. Temperature of PALT excluding MLI and PCB elements.

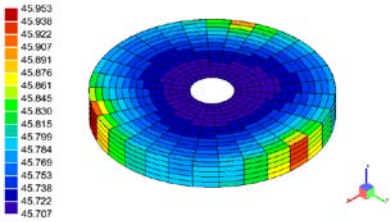

Figure 11. Temperature variation of Primary Mirror.

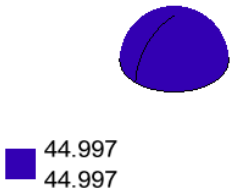

Figure 12. Temperature of APD.

Higher temperatures are however observed in the MLI cover but the optical and electronic components are within the safe temperature limits.

A safety margin of $\pm 15℃$ was added to the results obtained by the simulation. The electronic elements (those dissipating power of the PCB) were analyzed in detail, considering their respective survival temperatures, and they are all compliant. Figure 10 shows the PALT temperature that is compared with the qualification temperature limits, which is, $-50℃ < PALT < 70℃$. Considering the safety margin of $\pm 15℃$, PALT is going to have a temperature range of $25.075℃ < PALT < 67.056℃$, which is complaint with the requirements. For the Hot operational case, the primary mirror is going to have a temperature range of $60.707℃ < M1 < 60.953℃$, and the APD is going to have a maximum temperature of $59.997℃$. The operational temperature limits established by the APD supplier are within the range of $-50℃$ and $+ 80℃$, which is not exceeded in the simulation. Regarding the primary mirror, the main concern was the temperature range along its surface, and since the maximum and the minimum values differ less than $1℃$, it can be stated that the mirror will survive in the hot operational use case.

The thermoelastic design was subjected to multiple iterations to be compliant with the acceptance tolerances that are presented in Table 1. The major design change was relatively to the electronics box.

From the first simulations, with the box design as shown in Figure 4, it was possible to detect a high deformation of the box lid, where the instrument is based upon, and consequently the possibility of affecting the optical performance. Updating the box design for the design shown in Figure 5, the optical tolerances can be achieved. Only the hottest operational case with 15° of solar angle and the cold operational with 0° of solar angle case were simulated. The results are presented in Figure 13 and Table 3. The boundary conditions applied to this model were a fixed support on a vertex a free displacement along the x and z axis on the bottom surface of the S/C. This last boundary condition was applied due to the base small dimensions, that consequently was reflected in a noticeable base deformation, affecting the remain box deformation results.

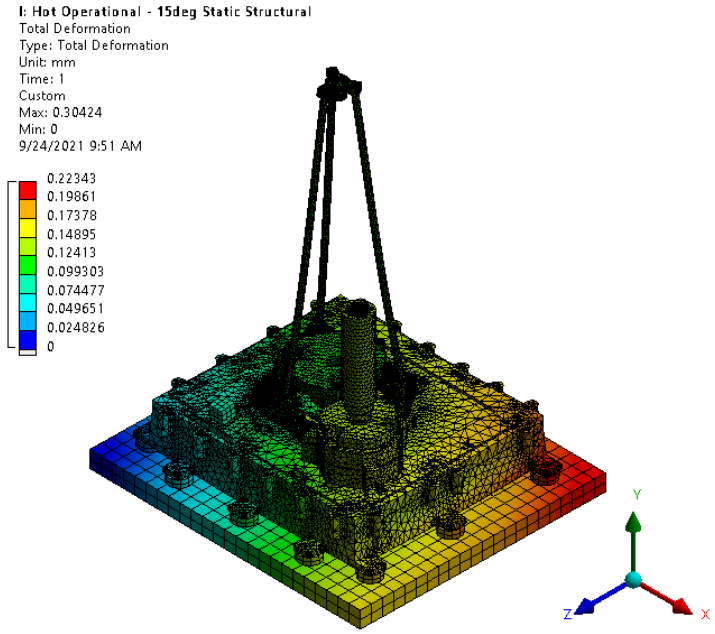

Figure 13. Thermoelastic total deformation of hot operational case.

The thermoelastic simulation regarding the total deformation was calculated in detail for the tolerance study.

Table 3. Thermal operation tolerances

	M1 tilt (mrad)	M1 and M2 distance (mm)	M2 tilt (mrad)	Telescope vs emitter (mrad)
Maximum admissible thermal operation tolerances (i.e., requirements for the thermal elastic deformation)	∓0.03	∓0.05	∓0.05	∓0.15
Hot operational case 15° solar angle	0.0046	0.01318	0.000873	0.299

The tolerance for the angle between the telescope and the emitter is not compliant. However, according to the radiometric calculations, this value is still inside the margin of signal to noise ratio, which is reflected in a loss of 10% of energy.

5. Conclusion

The PALT design included several design changes that resulted on a relationship between thermal design and optical design. The electronics box design is still under optimization, however, since the

requirements have been already achieved, this model is considered the worst-case scenario. The maximum admissible thermal operation tolerances regarding M1 and M2 tilt and distance between mirrors were achieved, apart from the angle between the telescope and the emitter, which result in a maximum of 10% loss of energy.

Regarding the thermal model, the results are within the acceptable values, both for the electronics. The APD is within the limit range of temperatures establish by the supplier, and for the optical elements, the primary mirror have a narrow range of temperature on its surface, assuring its survival and operation. The HERA LIDAR design demonstrated to be up to the requirements established for the mission, maintaining its compact design and its operational performance.

Acknowledgment

The authors would like to thank NEO-MAPP Team: Karl Atkinson, Paula Benavidez, Jens Biele, Mélanie Drilleau, Colleen Fiaschetti, Sarah Fontaine, Alain Hérique, Martin Jutzi, Ozgur Karatekin, Julia de Leon, Javier Licandro, Naomi Murdoch, Danica Rémy, Grig Richter, Francisco da Silva Pais Cabral, Paolo Tortora, Kleomenis Tsiganis, JeanBaptiste Vincent, George Voyatzis, Kai Wuennemann, Marco Zannoni (https://neomapp.eu/team-new). This work has received funding from the European Union's Horizon 2020 research and innovation programme under grant agreement No 870377 (project NEO-MAPP); funded through Foundation for Science and Technology (FCT) under the ICT project UIDP/04683/2020; Portuguese Funds through the Foundation for Science and Technology (FCT) under the LAETA project UIDB/50022/2020.

References

[1] Cheng A, Rivkin A, Michel P, Atchison J, Barnouin O, Benner O, Chabot N, Ernst C, Fahnestock E, Kueppers M and Pravec P 2018 *Planetary and Space Science* **157** 104-115.
[2] Gardner C 1992 *IEEE Transactions on Geoscience and Remote Sensing* **30(5)** 1061-1072.
[3] Tsuno K, Okumura E, Katsuyama Y, Mizuno T, Hashimoto T, Nakayama M and Yuasa H 2006 *International Society for Optics and Photonics* **10567** 105670W.
[4] Ramos-Izquierdo L, Scott V, Schmidt S, Britt J, Mamakos W, Trunzo R, Cavanaugh J and Miller R 2005 *Applied Optics* **44(9)** 1748-1760.
[5] Ramos-Izquierdo L, Scott III V, Connelly J, Schmidt S, Mamakos W, Guzek J, Peters C, Liiva P, Rodriguez M, Cavanaugh J and Riris H 2009 *Applied Optics* **48(16)** 3035-3049.
[6] Mizuno T, Kase T, Shiina T, Mita M, Namiki N, Senshu H, Yamada R, Noda H, Kunimori H, Hirata N and Terui F 2017 *Space Science Reviews* **208(1-4)** 33-47.
[7] Daly M G, Barnouin O S, Dickinson C, Seabrook J, Johnson C L, Cunningham G, Haltigin T, Gaudreau D, Brunet C, Aslam I and Taylor A 2017 *Space Science Reviews* **212(1)** 899-924.
[8] Dias N G, Arribas B N, Gordo P, Sousa T, Marinho J, Melicio R and Amorim A 2020 *IOP Conference Series: Materials Science and Engineering* **1024 (2021) 012112** 1-7.
[9] Dias N G, Nadal Arribas B, Gordo P, Sousa T, Marinho J, Melicio R, Amorim A and Michel P 2021 *Aircraft Engineering and Aerospace Technology* **93(6)** 1018-1028.